G. Zhou, Y. Ye, J. Wang, W. Zuo, Y. Fu, X. Zhou 2018. "Modeling Air-to-Air Plate-Fin Heat Exchanger without Dehumidification". Applied Thermal Engineering, 143, pp. 137-148. DOI: 10.1016/j.applthermaleng.2018.07.064.

Modeling air-to-air plate-fin heat exchanger without dehumidification

G.Zhou[1,2] Y.Ye[3] J.Wang[3] W.Zuo[3] Y.Fu[3] X.Zhou[1*]

[1] Academy of Building Energy Efficiency, Guangzhou University, Guangzhou, Guangdong 510006, China
[2] Tianhe College of Guangdong Polytechnic Normal University, Guangzhou, Guangdong 510540, China
[3] Department of Civil, Environmental and Architectural Engineering, University of Colorado Boulder, Boulder, CO 80309, USA
**Corresponding author. E-mail addresses: zhou_xiaoqing03@163.com*

Abstract

In heating, ventilation and air-conditioning (HVAC) systems, air-to-air plate-fin heat exchangers (PFHEs) can be used as heat recovery devices to reduce the building energy consumption. However, existing heat exchanger models have limitations in simulating the performance of air-to-air PFHEs. For example, some models adopt heat transfer correlations which are not suitable for PFHEs, while others require detailed geometric data which are usually difficult to access, etc. To address these limitations, we developed a new model for air-to-air PFHE without dehumidification. Based on empirical correlations dedicated to air-to-air PFHEs, the mathematical models of the heat transfer and the flow resistance were built. The new model considers the impacts of the changing air flow rates and temperatures. Additionally, it only requires readily available nominal parameters as inputs and does not need any geometric data. Furthermore, no numerical discretization is needed to solve the equations, which makes the model computationally more efficient than models using the finite-element method. To evaluate the performance of the new model, it is implemented using an object-oriented, equation-based modeling language Modelica. Case studies show that the new model can predict the results with a relative deviation less than 10% compared to the experimental data.

Key words: plate-fin heat exchanger, air-to-air, mathematical model, Modelica

Nomenclature

A	total heat transfer area, m^2	U	overall heat transfer coefficient, $W/(m^2K)$
A_f	fin area, m^2	u	characteristic velocity, m/s
A_{min}	minimum flow area, m^2	V	air velocity, m/s
c_p	specific heat capacity under constant pressure, $J/(kgK)$	x	factor for thermal variation of fluid properties in heat transfer module, dimensionless
$\dot{C}$	capacity rate, $J/(Ks)$		
C	constant	x_f	factor for thermal variation of fluid properties in flow resistance module, dimensionless
c	constant		
D_h	hydraulic diameter, m		
D_P	pressure drop, Pa	*Greek letters*	
e	relative error	Δ	Difference
f	friction factor, dimensionless	ε	heat transfer effectiveness, dimensionless
h	convective heat transfer coefficient, $W/(m^2K)$	ζ	pressure loss coefficient, dimensionless
		η	efficiency, dimensionless
j	heat transfer factor, dimensionless	ϑ	non-dimensional temperature
K	Constant or the unit of temperature	λ	thermal conductivity, $W/(mK)$
k	constant	μ	dynamic viscosity, $Pa \cdot s$
L	characteristic length, m	ρ	density, kg/m^3
L_P	louver pitch, m	χ	ratio of x under a special condition, dimensionless
$\dot{m}$	mass flow rate, kg/s		
m	exponent of Reynolds number in the correlation of heat transfer factor	φ	imbalance rate of heat transfer rates of both sides
n	exponent of Reynolds number in the correlation of Nusselt number		*Subscripts*
		0	nominal condition
N	exponent of Reynolds number in the correlation of the friction factor	1	side 1 of heat exchanger or subscript of constant

NTU	number of heat transfer units, dimensionless	2	side 2 of heat exchanger or subscript of constant
Nu	Nusselt number, dimensionless	c	the abrupt narrowing of the circulation area
P	total pressure, Pa	e	the abrupt widening of the circulation area
Pr	Prandtl number, dimensionless	f	fin
$\dot{Q}$	heat transfer rate, W	i	side number of heat exchanger
R	ideal gas constant, $J/(kgK)$	in	inlet
R_c	capacity rate ratio, dimensionless	max	maximum
Re	Reynolds number, dimensionless	min	minimum
r	ratio of convective heat transfer coefficients, dimensionless	out	outlet
		t	total
T	temperature, K		

1 Introduction

The building sector is under pressure to improve its overall energy efficiency due to its colossal energy demand [1]. Advanced energy-efficient Techniques (e.g. heat recovery, grounded source heat pump) draw more attentions [2, 3]. In HVAC systems, air-to-air plate-fin heat exchangers (PFHEs) can be used as heat recovery devices to reduce the building energy consumption. The plate-fin heat exchanger (PFHE) is a compact heat exchanger that consists of a stack of alternating plates called parting sheets, and fins brazed together as a block [4, 5]. Fig. 1 shows the structure of a typical PFHE. Common PFHE fin types are: plain fin, wavy fin, offset fin and louvered fin etc. [6] An existing study [7] compares the performance of different plate-fin channels, which can be taken as a reference to the optimal design of the PFHEs. PFHE has some advantages over other kinds of heat exchangers. For example, it has close temperature approaches, high thermal effectiveness, a large heat transfer area per unit volume (typical $1000\ m^2/m^3$), a low weight per unit transfer, and the capability of heat exchange between many process streams [4]. For these reasons, air-to-air PFHEs have been used in building HVAC systems as high-efficient energy recovery devices. A study [8] shows that using air-to-air PFHEs in the HVAC system for heat recovery can lead to great energy saving, as the load of the fresh air handling unit is reduced by *45% ~ 70%*. Besides, since the fresh air and exhaust air do not have contact with each other, there is no cross contamination between them, which will benefit the indoor air quality.

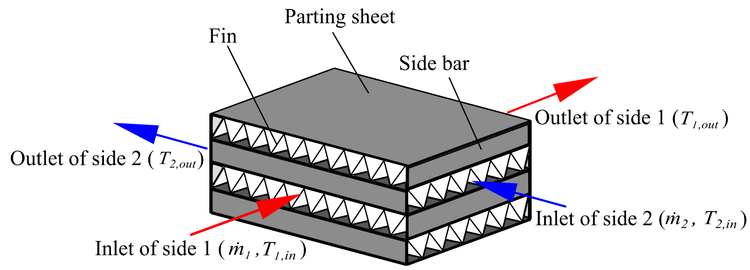

Fig. 1 Diagram of the structure of a PFHE

A review of existing air-to-air heat exchanger models from the literature and mainstream simulation platforms shows that they have limitations in the modeling of air-to-air PFHEs. Wetter [9] presented a simple simulation model of an air-to-air plate heat exchanger with effectiveness-NTU method. However, Wetter's model is designed for plate heat exchangers and calculates the convective heat transfer coefficient based on an empirical correlation with a fixed exponent of velocity, which makes it not applicable for the PFHEs. Nakonieczny [10] described a numerical model of the air-to-air PFHE under unsteady flow conditions. In this model, geometric parameters of the heat exchanger are needed, which are usually difficult to access. The unsteady-flow equations in this model are discretized with a semi-discrete finite-element method, which can lead to a longer computational time and may cause difficulties in achieving convergence. Rose, Nielsen, Kragh and Svendsen [13] and Nielsen, Rose and Kragh [14] presented a quasi-steady-state model and a dynamic model of a counter-flow air-to-air heat exchanger, respectively. In these two models, the effects of dehumidification and frost formation are taken into account and geometric data are needed in the calculation of the Reynolds number. Similarly, Liu, Rafati Nasr, Ge, Justo Alonso, Mathisen, Fathieh and Simonson [15] developed a theoretical model to predict frosting limits for cross-flow air-to-air heat exchangers, which needs geometric data for the calculation of the heat transfer coefficient.

As for the mainstream simulation platforms, in Modelica Buildings Library [16], the heat exchanger model *Fluid.HeatExchangers.ConstantEffectiveness* can simulate air-to-air heat transfer, but it uses constant heat effectiveness ε without considering the impacts of changing air flow rates and temperatures. In EnergyPlus[17], there are three air-to-air heat exchanger simulation models. The model *Air-To-Air Sensible and Latent Effectiveness Heat Exchanger* models a full heat exchanger, which is different from PFHE in structure and material. The *Air-To-Air Flat Plate Heat Exchanger* model adopts Wetter's model [9] mentioned above. The *Balanced Flow Desiccant Heat Exchanger* model is dedicated for desiccant heat exchangers, which is also different from PFHE. In the Standard Component Library of TRNSYS 17 [18], *Type 5* and *Type 91* can be used in the modeling of air-to-air heat exchangers. The heat transfer effectiveness ε of *Type 5* is calculated based on a fixed overall heat transfer coefficient UA. *Type 91* uses a constant effectiveness. In the Standard Component Library of TRNSYS 18 [19], no new air-to-air heat exchanger model is developed. In TESS Library 17 [20], *Types 512*, *650*, *652*, *657*, *667, 699*, *760,* and *761* can be used to model air-to-air heat exchangers, but all of them use constant heat transfer effectiveness. However, almost all the above-mentioned models do not involve the calculation of flow resistance, except for the model in Modelica Buildings Library. Since the flow resistance directly affects the power consumption of the fluid machines in HVAC systems [16, 21], it should be included as part of the heat exchanger modeling. In the flow resistance calculation of the model in Modelica Buildings Library, the relationship between pressure drop ΔP and mass flow rate $\dot{m}$ is quadratic [21], which is not consistent with the situation in PFHEs. Investigations [5, 6, 22] show that the correlation of the friction factor f in different PFHEs can be generally written as $f = k_1 k_2 Re^N$. From this correlation, we cannot derive the relationship between pressure drop ΔP and mass flow rate $\dot{m}$ is quadratic in PFHEs.

To sum up, the following limitations of existing models in the modeling of air-to-air PFHEs are noticed:

- Needing detailed geometric data of the heat exchanger that are seldom accessible.
- Using the finite-element method, which leads to longer computational time and difficulties in achieving convergence.
- Using the constant heat transfer effectiveness ε or fixed overall heat transfer coefficient UA without considering the impacts of the changing conditions on heat transfer.
- Using an inapplicable correlation between the pressure drop and the mass flow rate for PFHEs.

In this paper, we present a new model for air-to-air PFHEs that overcomes the above-mentioned limitations of existing models. The new model adopts correlations of the heat transfer factor and the friction factor that are based on PFHEs, which makes the calculation results of heat transfer and pressure drop closer to real cases. As input, it only needs nominal data that are available during the design phase of HVAC systems to calculate the heat transfer coefficients. This avoids the difficulty of getting access to geometric data of the heat exchanger. Only explicit equations are used in the model to avoid numerical discretization as needed by the finite-element method. In this way, short computational time and numerical stability are ensured. Also, the impact of the changing air flow rate and temperature on the convective heat transfer coefficient is considered. The new model can be used to calculate both the heat transfer and the flow resistance. In the present stage of our work, we only focus on modeling air-to-air PFHEs without dehumidification. The effects of dehumidification will be considered in the future work.

Fig. 2 shows the methodology of this paper. At first, the mathematical model of the PFHE is abstracted according to its physical properties. The flow resistance correlation and the heat transfer correlation of the PFHE are chosen from literature, based on which the two mathematical modules, heat transfer module and flow resistance module, are established. After that, we implemented the mathematical model using the object-oriented, equation-based modeling language Modelica. Then, experimental data from literature are used to evaluate the two modules, respectively. At last, simulation results are analyzed and concluding remarks of this paper are made.

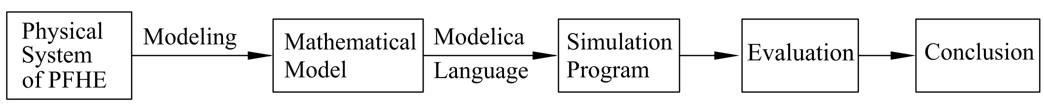

Fig. 2. Methodology of the work in this paper

2 Mathematical Model Description

2.1 General Description

In this paper, it is assumed that the geometric structure and dimension on both sides of the heat exchanger are the same. Given this assumption, the heat transfer correlations on both sides are the same, as well as the flow resistance correlations. Fig. 1 is a schematic diagram of sides 1 and 2 of the heat exchanger.

The mathematical model consists of a heat transfer module and a flow resistance module. They are independent of each other. The new model can predict the performance of the air-to-air PFHE under non-nominal conditions based on the performance under the nominal condition. The nominal data are available in the design phase of an HVAC system. Besides, the mass flow rate and inlet air temperature under non-nominal conditions on each side of the heat exchanger are also measurable. Based on these known variables, we can get those unknown variables under non-nominal conditions; namely, the heat transfer rate, the pressure drop, and the outlet temperature. Here, the nominal condition is decided by users during the design phase. It can be the design condition, the maximum load condition, or measured catalog data provided by the manufactures. Considering the selection of the nominal data may affect the calculation results under non-nominal conditions, we propose using the catalog data from manufacturers, which are often available in the design phase. In the following part, the detailed description of the mathematical models for heat transfer and flow resistance are presented.

2.2 Detailed Model Description

2.2.1 Heat Transfer Module

In the mathematical calculation of the heat transfer module, the following assumptions are made: 1) The fouling and thema1 resistance of the material are neglected; 2) No leakage of airflow or heat loss to the environment occur; 3) The air pressure is considered approximately 1 bar; 4) The specific heat capacity and Prandtl number of air and the fin efficiency are constant; 5) The model is static.

The following mathematical derivation of heat transfer adopts the effectiveness-NTU method [23]. Here, the dimensionless heat transfer effectiveness ε is defined as the actual heat transfer $\dot{Q}$ divided by the possibly maximum heat transfer $\dot{Q}_{max}$:

$$\varepsilon = \frac{\dot{Q}}{\dot{Q}_{max}}. \tag{1}$$

For most single channel counter flow heat exchangers, the heat transfer effectiveness ε lies between 50% and 70% [24]. The actual heat transfer can be expressed as:

$$\dot{Q} = \dot{C}_1 \left| T_{1,out} - T_{1,in} \right| = \dot{C}_2 \left| T_{2,in} - T_{2,out} \right|, \tag{2}$$

where T is inlet temperature or outlet temperature of two sides of the heat exchanger, and $\dot{C}$ is the capacity flow and is the product of mass flow rate $\dot{m}$ and specific heat capacity of air c_p:

$$\dot{C} = \dot{m} c_p. \tag{3}$$

The possibly maximum heat transfer rate is:

$$\dot{Q}_{max} = \dot{C}_{min} \left| T_{2,in} - T_{1,in} \right|, \tag{4}$$

where $\dot{C}_{min}$ is the lower capacity rate of both streams:

$$\dot{C}_{min} = min(\dot{C}_1, \dot{C}_2)\ . \tag{5}$$

Substituting *Eq. (2)* and *Eq. (4)* into *Eq. (1)*, the ε can be written as:

$$\varepsilon = \frac{\dot{C}_1 \left(T_{1,in} - T_{1,out} \right)}{\dot{C}_{min} \left(T_{1,in} - T_{2,in} \right)}. \tag{6}$$

The dimensionless number of heat transfer units (*NTU*) is defined as:

$$NTU = \frac{UA}{\dot{C}_{min}}, \tag{7}$$

where U is overall heat transfer coefficient, A is total heat transfer area.

The correlation between ε and *NTU* is:

$$\varepsilon = f(NTU, R_C, flow\ arrangement), \tag{8}$$

where R_C is the dimensionless capacity rate ratio:

$$R_C = \frac{\dot{C}_{min}}{\dot{C}_{max}}. \tag{9}$$

Different variations of *Eq.(8)* according to the flow arrangement are listed in Table 1. Only two common configurations of the heat exchanger are considered here: counter flow and cross flow. For the cross flow, both streams mixed and both streams unmixed are considered. For plain fin and wavy fin PFHEs, it is both streams unmixed, while for offset fin and louvered fin PFHEs, it is both streams mixed.

Table 1. Correlations between ε and NTU for different heat exchanger flow arrangements [17]

Flow arrangement	$\boldsymbol{\varepsilon = f(NTU, R_C, flow\ arrangement)}$	$\boldsymbol{NTU = f(\varepsilon, R_C, flow\ arrangement)}$
Counter flow heat exchanger	$\varepsilon = \frac{1 - exp[-NTU(1 - R_C)]}{1 - R_C exp[-NTU(1 - R_C)]}$	$NTU(R_C \neq 1) = \frac{1}{R_C - 1}\ln(\frac{1 - \varepsilon}{1 - \varepsilon R_C})$ $NTU(R_C = 1) = \frac{\varepsilon}{1 - \varepsilon}$
Cross flow heat exchanger with both streams unmixed	$\varepsilon = 1 - exp\left\{\frac{NTU^{0.22}}{R_C}[exp(-R_C NTU^{0.78}) - 1]\right\}$	$NTU = f(\varepsilon, NTU, R_C)$ The solution is unique [25].
Cross flow heat exchanger with both streams mixed	$\varepsilon = \left[\frac{1}{1 - exp(-NTU)} + \frac{R_C}{1 - exp(-R_C NTU)} - \frac{1}{NTU}\right]^{-1}$	$NTU = f(\varepsilon, NTU, R_C)$ The solution is unique.

If the effectiveness ε is known, according to *Eq.(6)*, the outlet temperature of side 1 can be calculated with:

$$T_{1,out} = T_{1,in} + \varepsilon \frac{\dot{C}_{min}}{\dot{C}_1}\left(T_{2,in} - T_{1,in}\right). \tag{10}$$

The heat transfer rate then becomes:

$$\dot{Q} = \dot{C}_1(T_{1,out} - T_{1,in}). \quad (11)$$

The outlet temperature of side 2 is:

$$T_{2,out} = (T_{2,in} - \frac{\dot{Q}}{\dot{C}_2}). \quad (12)$$

Using *Eq.(1)*, *Eq. (3)*, *Eq. (4)* and *Eq. (5)* with nominal data $T_{1,in,0}$, $\dot{m}_{1,0}$, $T_{2,in,0}$, $\dot{m}_{2,0}$ and $\dot{Q}_0$, we can get ε_0. Then, using *Eq. (8)* and *Eq. (9)*, we can get NTU_0. Finally, using *Eq. (7)*, we can get $(UA)_0$ as:

$$(UA)_0 = NTU_0 \dot{C}_{min,0}. \quad (13)$$

Next, we will determine the convective heat transfer coefficient of both sides and overall heat transfer coefficient of heat exchanger under non-nominal conditions.

Under non-nominal conditions, when neglecting the heat resistance of the material and the fouling on the surface, the overall heat transfer coefficient *UA* is calculated as [24]:

$$UA \approx \frac{1}{\left(\frac{1}{\eta_t hA}\right)_1 + \left(\frac{1}{\eta_t hA}\right)_2}, \quad (14)$$

where h is the convective heat transfer coefficient, η_t is the total fin efficiency[23]:

$$\eta_t = 1 - \left(1 - \eta_f\right)\frac{A_f}{A}. \quad (15)$$

In *Eq.(15)*, A_f is the area of fins, *A* is the total heat transfer area and η_f is the fin efficiency.

The ratio *r* is defined as the quotient of the convective heat transfer coefficients over the two sides of the heat exchanger under nominal condition:

$$r = \frac{(\eta_t hA)_{1,0}}{(\eta_t hA)_{2,0}}. \quad (16)$$

Using *Eq.(14)* and *Eq. (16)*, the $(\eta_t hA)_{i,0}$ value under nominal conditions can be written as:

$$(\eta_t hA)_{1,0} = (r+1)(UA)_0, \quad (17)$$

and

$$(\eta_t hA)_{2,0} = \frac{(r+1)}{r}(UA)_0. \quad (18)$$

As the next step, the $(\eta_t hA)_i$ under non-nominal conditions is calculated, based on which the total heat transfer coefficient *UA* under non-nominal conditions is further obtained using *Eq.(14)*.

Based on the literature [5, 6, 22, 26-35], the correlation of heat transfer factor j for different PFHEs can be written as:

$$j = c_1 c_2 Re^m \,, \tag{19}$$

where c_1 is a constant real number, c_2 is a constant that only depends on the geometry of the heat exchanger, m is the exponent of Reynolds number Re .The definition of j is:

$$j = \frac{Nu}{RePr^{1/3}} \,, \tag{20}$$

where Nu is Nusselt number, Re is Reynolds number and Pr is Prandtl number.

The definition of Re is:

$$Re = \frac{\rho u L}{\mu} \,, \tag{21}$$

where ρ is the density of air, u is the characteristic velocity, L is the characteristic length and μ is the dynamic viscosity. The characteristic temperature used here is the average of the inlet and outlet temperatures of the heat exchanger. For different types of fins, the characteristic length L is different. For plain fin, wavy fin and offset fin, it is the hydraulic diameter D_{h} at the fin inlet, while for louvered fin, it is usually the louver pitch L_P. The characteristic velocity u of PFHE is defined as the maximum velocity between the fins and is similar to the average velocity in the constant flow section [36]:

$$u = \frac{\dot{m}}{\rho A_{min}} \,, \tag{22}$$

where A_{min} is the minimum flow area.

The definition of Nusselt number Nu is as following:

$$Nu = \frac{hL}{\lambda} \,, \tag{23}$$

where λ is the thermal conductivity.

Using *Eq. (19)* and *Eq.(20)*, Nu can be rewritten as:

$$Nu = c_1 c_2 Pr^{1/3} Re^{m+1}. \tag{24}$$

The air temperature in an HVAC system usually lies from 278.15 K to 318.15 K. In this range, the value of Prandtl number Pr varies very little [37]. Hence, Pr in this paper is regarded as a constant.

Let $C = c_1 c_2 Pr^{1/3}$ and $n = m + 1$, then *Eq.(24)* can be written as:

$$Nu = CRe^n\ . \tag{25}$$

Table 2 lists some correlations of heat transfer factor j for different fin types and the corresponding exponent values for the calculation of Nu. Based on the literature [5, 6, 22, 26-35], the range of m lies between -1 and 0 and the range of n between 0 and 1. When choosing the value of m or n without sample data or test data at hand, special attention should be paid to the following aspects: 1) The form of the correlation should be as in *Eq.(19)* or *Eq.(25)* and corresponding to the type of fin. 2) Even for the same type of fin, there exist different correlations, which should be further chosen according to the characteristics of the equipment. 3) The range of Reynolds number should match that of the correlation. 4) When calculating the Reynolds number, the characteristic length should match the fin type. However, in the design phase, it is usually difficult to get detailed geometric data of the equipment, such as the channel cross-sectional flow area. This makes the calculation of Reynolds number difficult. Therefore, in this paper, we estimated the Reynolds number range according to the flow velocity and the type of product. Then, we chose the corresponding heat transfer factor correlation from Table 2. When sample data or test data of the product are available, further modification of m or n is possible.

Table 2. Correlations of heat transfer factor j for different fin types

Fin type	$\boldsymbol{j}$	$\boldsymbol{m}$	$\boldsymbol{n = m + 1}$	**Range of** $\boldsymbol{Re}$	**References**
Plain fin	$j = 0.271c_2Re^{-0.3345}$	-0.3345	0.6655	$600 \le Re \le 8000$	[6]
Wavy fin	$j = 0.0836c_2Re^{-0.2309}$	-0.2309	0.7691	$600 \le Re \le 7000$	[6, 33]
	$j = 0.0482c_2Re^{-0.23725}$	-0.23725	0.76275	$600 \le Re \le 7000$	[34]
	$j = 0.2951c_2Re^{-0.1908}$	-0.1908	0.8092	$Re < 1900$	[35]
	$j = 0.7293c_2Re^{-0.3637}$	-0.3637	0.6363	$Re \ge 1900$	
Offset fin	$j = 0.483c_2Re^{-0.536}$	-0.536	0.464	$Re \le 1000$	[38]
	$j = 0.242c_2Re^{-0.368}$	-0.368	0.632	$Re \ge 2000$	
Louvered fin	$j = 0.436c_2Re_{Lp}^{-0.559}$	-0.559	0.441	$100 \le Re_{Lp} \le 1000$	[26]
	$j = 0.26712c_2Re_{Lp}^{-0.1944}$	-0.1944	0.8056	$200 \le Re_{Lp} \le 2500$	[32]

Using *Eq. (25)*, the Nusselt number under non-nominal conditions can be written as:

$$\frac{Nu}{Nu_0} = (\frac{Re}{Re_0})^n , \tag{26}$$

where Nu_0 and Re_0 represent the Nusselt number and the Reynolds number under nominal conditions, respectively.

Substitute *Eq. (21)* and *Eq.(23)* into *Eq.(26)* , and the convective heat transfer coefficient under non-nominal conditions becomes:

$$\frac{h}{h_0} = \frac{\lambda}{\lambda_0}(\frac{u}{u_0}\frac{\rho}{\rho_0}\frac{\mu_0}{\mu})^n . \tag{27}$$

Substitute *Eq.(22)* into *Eq.(27)*:

$$\frac{h}{h_0} = \frac{\lambda}{\lambda_0}(\frac{\dot{m}}{\dot{m}_0}\frac{\mu_0}{\mu})^n . \tag{28}$$

Eq. (28) can also be written as:

$$\frac{h_i}{h_{i,0}} = x_i(T_i)(\frac{\dot{m}_i}{\dot{m}_{i,0}})^n , \tag{29}$$

where $i = 1, 2$ represents the two sides of the heat exchanger. $x_i(T_i)$ represents the air property under non-nominal conditions and is a function of the air temperature:

$$x_i(T_i) = \frac{\lambda_i}{\lambda_{i,0}}(\frac{\mu_{i,0}}{\mu_i})^n . \tag{30}$$

In HVAC systems, the air pressure usually lies around 1 bar. Dynamic viscosity μ of dry air under a pressure of 1 bar can be approximated linearly by [25]:

$$\mu = c_3 + c_4(T - 273.15) , \tag{31}$$

where $c_3 = 1.706 \times 10^{-5}$, $c_4 = 4.529 \times 10^{-8}$.

The thermal conductivity λ of dry air at 1 bar can be approximated linearly by [25]:

$$\lambda = c_5 + c_6(T - 273.15) , \tag{32}$$

where $c_5 = 2.453 \times 10^{-2}$, $c_6 = 7.320 \times 10^{-5}$.

Substitute *Eq.(31)* and *Eq. (32)* into *Eq. (30)*:

$$x_i(T_i) = \frac{c_5 + c_6(T_i - 273.15)}{c_5 + c_6(T_{i,0} - 273.15)}\left[\frac{c_3 + c_4(T_{i,0} - 273.15)}{c_3 + c_4(T_i - 273.15)}\right]^n . \tag{33}$$

We use first order Taylor series to expand the function of $x_i(T_i)$ in *Eq. (33)* with respect to the variable T_i at the temperature $T_{i,0}$. We select $T_{i,0} = 298.15K$, which is a median value in the range of air temperature in an HVAC system. Then, we get the approximated x_i:

$$x_i \approx 1 + (2.7769 \times 10^{-3} - 2.4895 \times 10^{-3} n)(T_i - T_{i,0}) . \quad (34)$$

Based on *Eq. (33)* and *Eq. (34)*, the relative error of x_i is:

$$e\_x_i = \frac{\left| \frac{c_5 + c_6(T_i - 273.15)}{c_5 + c_6(T_{i,0} - 273.15)} \left[\frac{c_3 + c_4(T_{i,0} - 273.15)}{c_3 + c_4(T_i - 273.15)} \right]^n - \left[1 + (c_7 - c_8 n)(T_i - T_{i,0}) \right] \right|}{\frac{c_5 + c_6(T_i - 273.15)}{c_5 + c_6(T_{i,0} - 273.15)} \left[\frac{c_3 + c_4(T_{i,0} - 273.15)}{c_3 + c_4(T_i - 273.15)} \right]^n} \times 100\% , \quad (35)$$

where $c_7 = 2.7769 \times 10^{-3}$, $c_8 = 2.4895 \times 10^{-3}$.

In HVAC systems, the air temperature T usually lies between 278.15 K and 318.15 K. For this temperature range, we calculated the maximum value of the relative error e_x_i for $n \in [0,1]$. As shown in Fig. 3, the maximum value of e_x_i varies in a range of 0.653%~0.034%. So, we can come to the conclusion that *Eq.(34)* approximates x_i with a good accuracy. To avoid iteration, the air property function x_i is calculated using the air inlet temperature rather than the mean air temperature [9]:

$$x_i \approx 1 + (2.7769 \times 10^{-3} - 2.4895 \times 10^{-3} n)(T_{i,in} - T_{i.in,0}) . \quad (36)$$

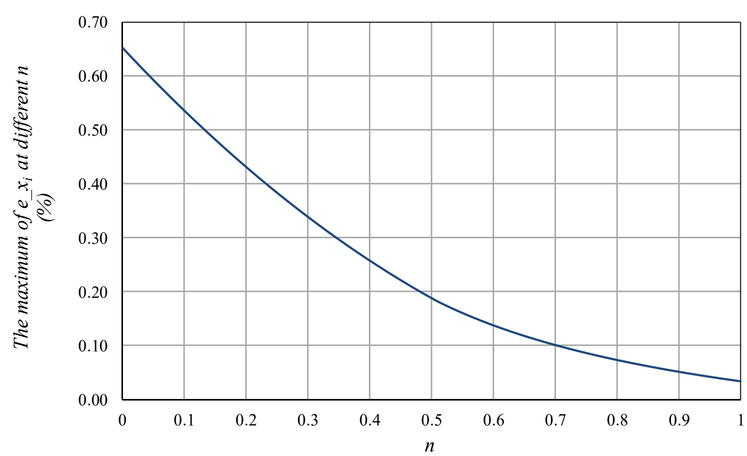

Fig. 3. Maximum value of e_x_i over n

According to *Eq. (29)*, we have:

$$(\eta_t hA)_i = x_i \left(\frac{\dot{m}_i}{\dot{m}_{i,0}}\right)^n (\eta_t hA)_{i,0} . \quad (37)$$

Using *Eq. (17)*, *Eq. (18)* and *Eq. (37)*, *Eq. (14)* can be rewritten as:

$$UA \approx \frac{(r+1)(UA)_{\,0}}{\frac{1}{x_1}(\frac{\dot{m}_{1,0}}{\dot{m}_1})^n + \frac{r}{x_2}(\frac{\dot{m}_{2,0}}{\dot{m}_2})^n} \,. \tag{38}$$

In *Eq. (38)*, only the ratio *r* of $(\eta_f hA)_{\,i,0}$ values under nominal conditions remains unknown.

Since the cross sections of the heat exchanger are the same on both sides, the $(\eta_f hA)_{\,i,0}$ values are equal if and only if the mass flows and air temperatures are the same [9]. This situation is represented by the superscript * in following equations.

Let:

$$\dot{m}^*_{1,0} = \dot{m}^*_{2,0} \,, \tag{39}$$

$$T^*_{1,0} = T^*_{2,0} \,, \tag{40}$$

consequently, we have:

$$(\eta_t hA)^*_{1,0} = (\eta_t hA)^*_{2,0} \,. \tag{41}$$

Using *Eq.(37)*, we have:

$$(\eta_t hA)^*_{1,0} = x^*_1 (\frac{\dot{m}^*_{1,0}}{\dot{m}_{1,0}})^n (\eta_t hA)_{\,1,0} \,, \tag{42}$$

and

$$(\eta_t hA)^*_{2,0} = x^*_2 (\frac{\dot{m}^*_{2,0}}{\dot{m}_{2,0}})^n (\eta_t hA)_{\,2,0} \,. \tag{43}$$

Using *Eq. (36)*, *Eq. (39)*, *Eq. (41)* ,*Eq. (42)* and *Eq. (43)*, *Eq. (16)* can be rewritten as:

$$r = \frac{x^*_2}{x^*_1}(\frac{\dot{m}_{1,0}}{\dot{m}_{2,0}})^n = \frac{1 + (c_7 - c_8 n)\left(T^*_{2,0} - T_{2,in,0}\right)}{1 + (c_7 - c_8 n)\left(T^*_{1,0} - T_{1,in,0}\right)}(\frac{\dot{m}_{1,0}}{\dot{m}_{2,0}})^n \,. \tag{44}$$

Let $\chi = \frac{x^*_2}{x^*_1}$, then:

$$\chi = \frac{1 + (c_7 - c_8 n)(T^*_{2,0} - T_{2,in,0})}{1 + (c_7 - c_8 n)(T^*_{1,0} - T_{1,in,0})} \,. \tag{45}$$

Let $T^*_{1,0} = T^*_{2,0} = 298.15K$, which is the median value of the air temperature in an HVAC system. Then, we get the approximated χ:

$$\chi \approx \frac{1 + (c_7 - c_8 n)\left(298.15 - T_{2,in,0}\right)}{1 + (c_7 - c_8 n)\left(298.15 - T_{1,in,0}\right)} \,. \tag{46}$$

Based on *Eq. (45)* and *Eq. (46)*, the relative error of χ is:

$$e\_\chi = \frac{\left| \frac{1 + (c_7 - c_8 n)\left(T_{2,0}^* - T_{2,in,0}\right)}{1 + (c_7 - c_8 n)\left(T_{1,0}^* - T_{1,in,0}\right)} - \frac{1 + (c_7 - c_8 n)\left(298.15 - T_{2,in,0}\right)}{1 + (c_7 - c_8 n)\left(298.15 - T_{1,in,0}\right)} \right|}{\frac{1 + (c_7 - c_8 n)\left(T_{2,0}^* - T_{2,in,0}\right)}{1 + (c_7 - c_8 n)\left(T_{1,0}^* - T_{1,in,0}\right)}} \times 100\% \,. \qquad (47)$$

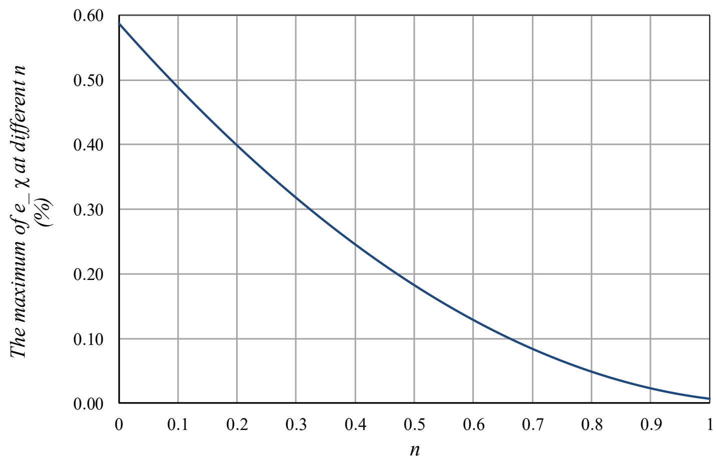

Fig. 4. Maximum value of e_χ over n

As mentioned before, the air temperature T in HVAC systems usually lies between 278.15 K and 318.15 K. For this temperature range, we calculated the maximum value of the relative error e_χ for $n \in [0,1]$. As shown in Fig. 4, the maximum relative error varies in a range of 0.588%~0.007%. So, we can conclude that *Eq. (46)* approximates χ with a good accuracy.

Thus, *Eq.(44)* can be rewritten as:

$$r = \frac{1 + (2.7769 \times 10^{-3} - 2.4895 \times 10^{-3} n)\left(298.15 - T_{2,in,0}\right)}{1 + (2.7769 \times 10^{-3} - 2.4895 \times 10^{-3} n)(298.15 - T_{1,in,0})} \left(\frac{\dot{m}_{1,0}}{\dot{m}_{2,0}}\right)^n . \qquad (48)$$

Then, using nominal inputs $\dot{m}_{1,0}$, $\dot{m}_{2,0}$, $T_{1,in,0}$, $T_{2,in,0}$, the values of r and $(UA)_0$ can be calculated. Finally, the UA values under non-nominal conditions are calculated with *Eq. (38).* As long as we know the UA values, we can get the heat transfer rate $\dot{Q}$ and outlet temperatures $T_{i,out}$ of both sides under non-nominal conditions with *Eq. (7) ~ Eq.(12)*.

Although the heat transfer module is based on heat transfer correlations of PFHEs, it could also be used in the modeling of other types of air-to-air heat exchangers if the following conditions are met. Firstly, two sides of the heat exchanger should have the same geometric structure and dimension, so that the same heat transfer correlation can be used. If not so, *Eq. (48)* cannot be derived. Secondly, the correlation of the heat transfer factor should have the following form: $j = c_1 c_2 Re^m$ or $Nu = CRe^n$ ($n = m + 1$). Thirdly, there should be no dehumidification during the heat transfer process.

2.2.2 Flow Resistance Module

Based on the literature [5, 6, 22, 28-31], the correlation of the friction factor f in different PFHEs can be written as:

$$f = k_1 k_2 Re^N , \tag{49}$$

where f is the friction factor, k_1 is a constant real number, k_2 is a constant that only depends on the geometry of the heat exchanger, and N is the exponent of Reynolds number Re.

Table 3 lists some correlations of the friction factor f and the corresponding N values for different fin types. Based on the literature [5, 6, 22, 28-31], N usually lies between -1 and 0. When choosing the value of N without sample data or test data at hand, special attention should be paid. For example, the form of the correlation should be as in *Eq. (*49*)*. Other considerations are similar to those when choosing the values of m and n in the heat transfer calculation.

Table 3. Correlations of friction factor f for different fin types

Fin type	$\boldsymbol{f}$	***N***	**Range of *Re***	**References**
Plain fin	$f = 3.479 k_2 Re^{-0.389}$	-0.389	$600 \le Re \le 8000$	[6]
Wavy fin	$f = 1.16 k_2 Re^{-0.309}$	-0.309	$600 \le Re \le 7000$	[6]
Offset fin	$f = 7.661 k_2 Re^{-0.712}$	-0.712	$Re \le 1000$	[38]
	$f = 1.136 k_2 Re^{-0.198}$	-0.198	$Re \ge 2000$	
Louvered fin	$f = k_2 Re_{Lp}^{-0.781}$	-0.781	$50 \le Re_{Lp} \le 500$	[28]

According to Dong [6], the friction factor *f* can be expressed as:

$$f = \left(\frac{A_{min}}{A}\right)\left(\frac{2\,\Delta P}{\rho u^2} - \zeta_c - \zeta_e\right), \tag{50}$$

where *A* is the total heat exchange surface area, A_{min} is the minimum flow area, ΔP is the pressure drop, ζ_c and ζ_e are the pressure loss coefficients caused by the abrupt narrowing and widening of the circulation area, respectively. Since ζ_c and ζ_e have little influence on the calculation of f [6], they can be ignored so that *Eq.(50)* can be further simplified as:

$$f = \left(\frac{A_{min}}{A}\right)\left(\frac{2\,\Delta P}{\rho u^2}\right). \tag{51}$$

According to *Eq.(21)*, *Eq. (22)*, *Eq.(49)* and *Eq. (51)*, we get:

$$\Delta P = 0.5 k_1 k_2 \left(\frac{A L^N}{{A_{min}}^{N+3}}\right)\frac{1}{\rho\,\mu^N}\dot{m}^{N+2}. \tag{52}$$

Let:

$$K = 0.5 k_1 k_2 \left(\frac{A L^N}{{A_{min}}^{N+3}}\right) = constant. \tag{53}$$

Then, *Eq.(52)* can be rewritten as:

$$\Delta P = K\frac{1}{\rho\,\mu^N}\dot{m}^{N+2}. \tag{54}$$

Based on *Eq.(54)*, the ratio of the pressure drops under non-nominal conditions ΔP to that under nominal condition ΔP_0 can be expressed as:

$$\frac{\Delta P}{\Delta P_0} = \frac{\rho_0}{\rho}\left(\frac{\mu_0}{\mu}\right)^N\left(\frac{\dot{m}}{\dot{m}_0}\right)^{N+2}. \tag{55}$$

For ideal gases, there is:

$$\rho = \frac{P}{RT}, \tag{56}$$

where P is the total pressure of air, R is the ideal gas constant, T is the air temperature.

Substitute *Eq.(56)* and *Eq.(31)* into *Eq(55)* and we get:

$$\frac{\Delta P_i}{\Delta P_{i,0}} = \frac{T_i}{T_{i,0}}\left[\frac{c_3 + c_4(T_{i,0} - 273.15)}{c_3 + c_4(T_i - 273.15)}\right]^N\left(\frac{\dot{m}_i}{\dot{m}_{i,0}}\right)^{N+2}, \tag{57}$$

where $i = 1, 2$ represents the two sides of the heat exchanger.

Let:

$$x_{f,i}(T_i) = \frac{T_i}{T_{i,0}}\left[\frac{c_3 + c_4(T_{i,0} - 273.15)}{c_3 + c_4(T_i - 273.15)}\right]^N, \tag{58}$$

where $x_{f,i}$ represents the air property as a function of the air temperature. Then *Eq.(57)* can be rewritten as:

$$\frac{\Delta P_i}{\Delta P_{i,0}} = x_{f,i} (\frac{\dot{m}_i}{\dot{m}_{i,0}})^{N+2} \,. \qquad (59)$$

We use first order Taylor series to expand the function of $x_{f,i}(T_i)$ in *Eq.(58)* with respect to the variable T_i at the temperature $T_{i,0}$. We select $T_{i,0} = 298.15K$, which is a median value in the range of the air temperature in an HVAC system. Then, we get the approximated $x_{f,i}$:

$$x_{f,i} \approx 1 + (3.3540 \times 10^{-3} - 2.4895 \times 10^{-3} N)\left(T_i - T_{i,0} \right) . \qquad (60)$$

Based on *Eq.(58)* and *Eq. (60)*, the relative error of $x_{f,i}(T)$ is:

$$e\_x_{f,i} = \frac{\left| \frac{T_i}{T_{i,0}} \left[\frac{c_3 + c_4(T_{i,0} - 273.15)}{c_3 + c_4(T_i - 273.15)} \right]^N - \left[1 + (c_9 - c_{10}N)\left(T_i - T_{i,0} \right) \right] \right|}{\frac{T_i}{T_{i,0}} \left[\frac{c_3 + c_4(T_{i,0} - 273.15)}{c_3 + c_4(T_i - 273.15)} \right]^N} \times 100\% \,, \qquad (61)$$

where $c_9 = 3.3540 \times 10^{-3}$, $c_{10} = 2.4895 \times 10^{-3}$.

In HVAC systems, the air temperature T often lies between 278.15 K and 318.15 K. For this temperature range, we calculated the maximum value of the relative error $e\_x_{f,i}$ for N∈ [-1, 0]. As shown in Fig. 5, the maximum value of relative error $e\_x_{f,i}$ lies in a range of 0.965%~3.619%. So, we can come to the conclusion that *Eq. (60)* approximates $x_{f,i}$ with a good accuracy. To avoid iteration, the air property $x_{f,i}$ is calculated using the air inlet temperature rather than the mean air temperature [9]. So, *Eq. (60)* can be rewritten as:

$$x_{f,i} \approx 1 + (3.3540 \times 10^{-3} - 2.4895 \times 10^{-3} N)(T_{i,in} - T_{i,in,0}) \,. \qquad (62)$$

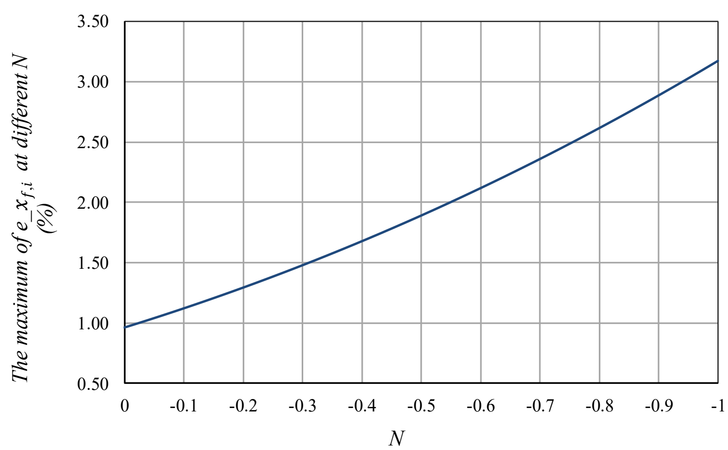

Fig. 5. Maximum value of $e\_x_{f,i}$ over N

In this way, the pressure drop ΔP_i under non-nominal conditions could be obtained using *Eq.(59)*, *Eq. (62)* and the inlet temperature $T_{i,in,0}$, the mass flow rate $\dot{m}_{i,0}$ and the pressure drop $\Delta P_{i,0}$ under nominal conditions.

Although the flow resistance module is based on the friction factor correlations of PFHEs, it could also be used in the modeling of other types of air-to-air heat exchangers, as long as the correlations have the following forms: $f = k_1 k_2 Re^N$ and $f = (A_{min}/A)(2\,\Delta P/\rho u^2)$.

3 Implementation of the New PFHE Model in Modelica

3.1 Introduction of Modelica and Modelica Buildings Library

Modelica is an equation-based, object-oriented modeling language. It is a new paradigm for building energy modeling, simulation, and optimization [39]. Compared to traditional building simulation programs, Modelica-based modeling and simulation have the following characteristics [40]: efficient numerical solution, good management of complex large systems, simulation of dynamic effects, use of models beyond time domain simulation, and use of models in conjunction with optimization algorithms. Due to these advantages, the new PFHE model is developed using Modelica.

Based on Modelica, Lawrence Berkeley National Laboratory (LBNL) developed the free open-source library Modelica Buildings Library [16]. This library supports rapid prototyping, as well as design and operation of building energy and control systems such as HVAC systems [16, 41-47]. It offers great convenience for users to implement building energy system modeling and simulation. The proposed air-to-air PFHE model without dehumidification is implemented based on this library.

3.2 Implementation of Air-to-Air PFHE

3.2.1 Structure of Model Implementation

Fig. 6 shows the hierarchical structure of the *Air-to-air PFHE* model. It consists of two main top-level blocks: the *hA* block and the *E-NTU* block. At the bottom-level of the model, there are four sub-blocks: *E-NTU calculator*, *Q-calculator*, *Static conservation equation* and *Flow resistance*. The combination of the *hA* block, *E-NTU calculator* sub-block, *Q-calculator* sub-block and *Static conservation equation* sub-block implements the function of the *heat transfer* module. While the *flow resistance* sub-block implements the function of the *flow resistance* module independently.

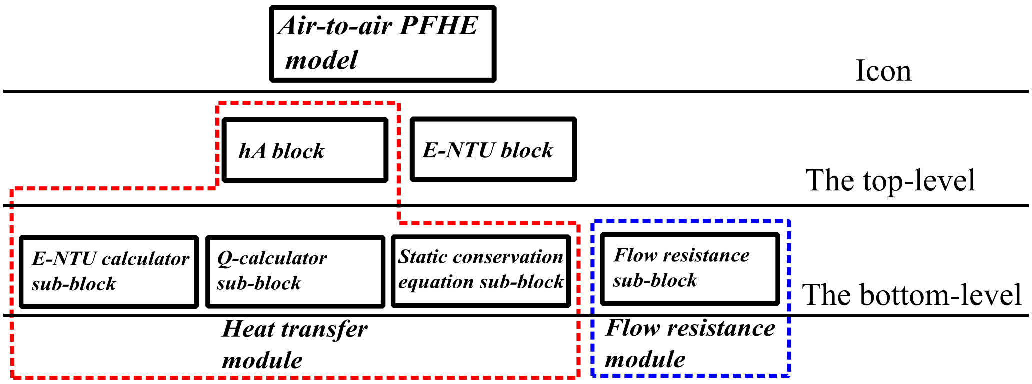

Fig. 6. Hierarchical structure of the Air-to-air PFHE model

Fig. 7 shows the icon and detailed top-level structure of the *Air-to-air PFHE* model in Modelica. The air inlets and outlets enable the connection of the PFHE model to an HVAC system. The two *mass flow rate sensor* blocks measure the mass flow rates $\dot{m}_1$ and $\dot{m}_2$, two *temperature sensor* blocks measure the inlet temperatures $T_{1,in}$ and $T_{2,in}$. These measurements are then exported to the *hA* block and the *E-NTU* block. The *hA* block is used to calculate the heat conductivities of two sides of the heat exchanger and exports the results to the *E-NTU* block. The function of the *E-NTU* block is to calculate UA, NTU, ε, $\dot{Q}$ and ΔP_i under non-nominal conditions.

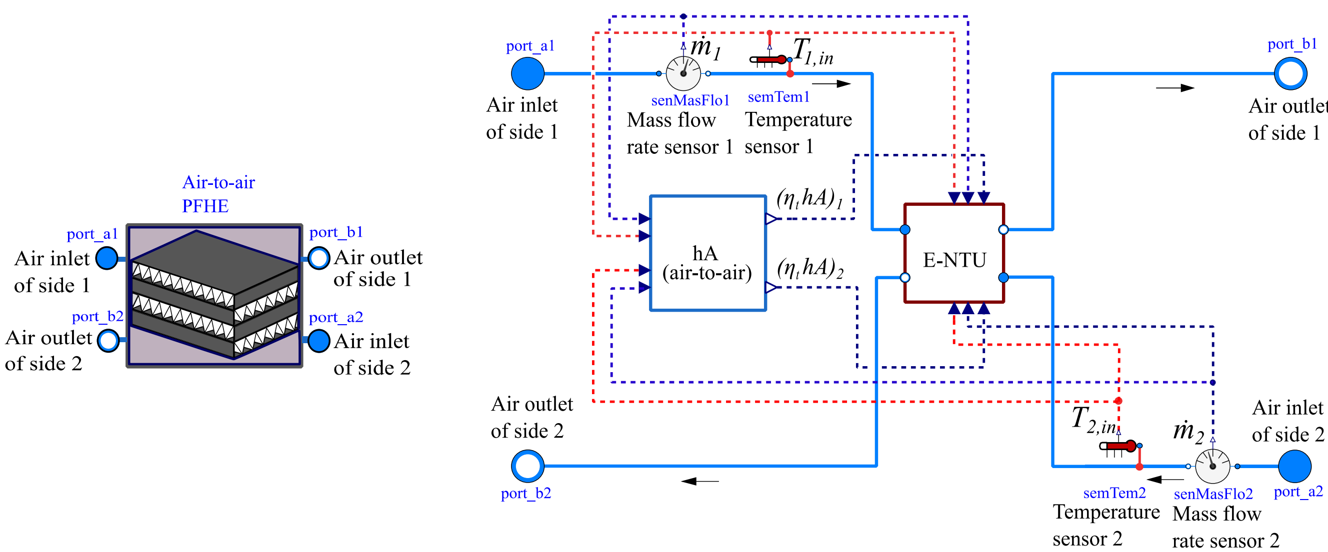

(a) Icon of the Air-to-air PFHE model
(b) Detailed top-level structure of the Air-to-air PFHE model

Fig. 7. Diagram of the air-to-air PFHE model in Modelica

Fig. 8 shows the detailed structure of the *E-NTU block*. There are four main sub-blocks: *E-NTU calculator*, *Q-calculator*, *Static conservation equation,* and *Flow resistance*, corresponding to the bottom-level of the hierarchical structure shown in Fig. 6. The *E-NTU calculator* sub-block is used to calculate UA, NTU and ε under non-nominal conditions. These results are then exported to the *Q-calculator* sub-block, which is used to calculate the heat transfer rate Q_i and outlet temperature $T_{out,i}$ on both sides of the heat exchanger. The heat transfer rate Q_i is imported into *Static conservation equation 1* and *Static conservation equation 2* sub-blocks. These blocks implement a steady-state conservation equation for energy and mass fractions and calculate the outlet variables of the heat exchanger. *Flow resistance 1* sub-block and *Flow resistance 2* sub-block are used to calculate the pressure drops ΔP_1 and ΔP_2 on both sides of the heat exchanger.

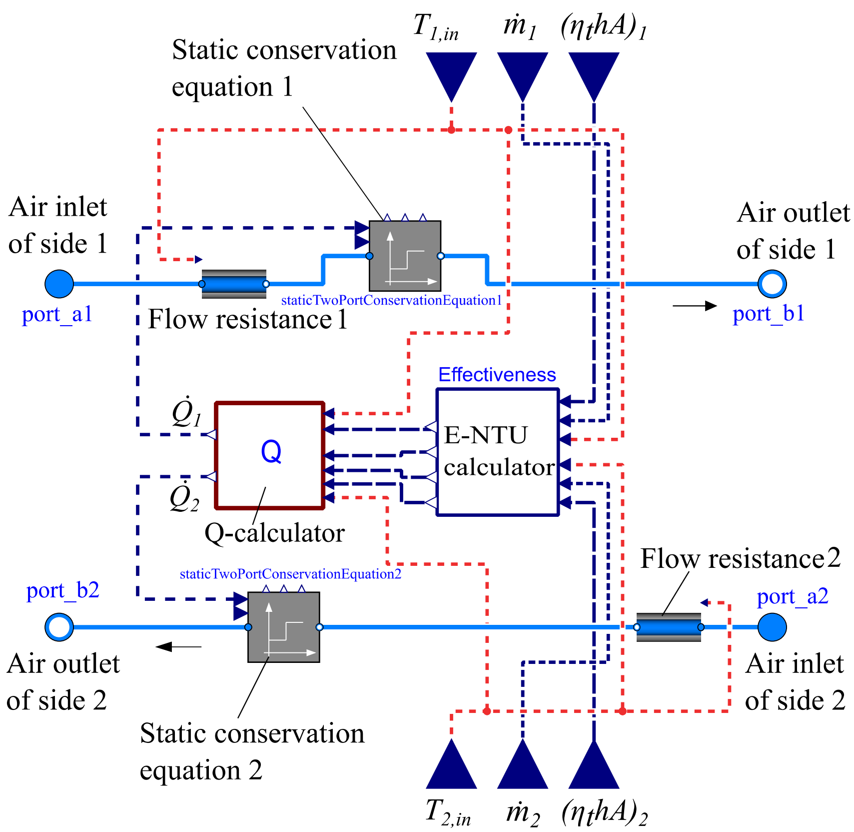

Fig. 8. Diagram of the E-NTU block in Modelica

3.2.2 Heat Transfer Module

As mentioned above, the *heat transfer* module is composed of the *hA* block, *E-NTU calculator* sub-block, *Q_calculator* sub-block and *Static conservation equation* sub-block (as Fig. 8). The combination of these blocks conducts the heat transfer calculation based on the mathematical model described in Section 2.2.1. The corresponding inputs, outputs, and applied equations of this module are listed in Table 4.

Table 4. Variables and equations of the heat transfer module

Parameters: $n\ (or\ m, n = m + 1), \dot{m}_{1,0}, \dot{m}_{2,0}, T_{1.in,0}, T_{2.in,0}, Q_0,\ flow\ arrangement$

Input variables: $T_{1,in}, T_{2,in}, \dot{m}_1, \dot{m}_2$

No.	Input	Equation	Output
1	$\dot{m}_{1,0}, \dot{m}_{2,0}, c_p$	*(3), (5)* and *(9)*	$\dot{C}_{1,0}, \dot{C}_{2,0,}\dot{C}_{min,0}, \dot{C}_{max,0}, R_{C,0}$
2	$\dot{C}_{min,0}, T_{1,in,0}, T_{2,in,0}$	*(4)*	$\dot{Q}_{max,0}$
3	$\dot{Q}_0, \dot{Q}_{max,0}$	*(1)*	ε_0
4	$\varepsilon_0, R_{C,0}, flow\ arrangement$	*(8)*	NTU_0
5	$NTU_0, \dot{C}_{min,0}$	*(7)*	$(UA)_0$
6	$n, T_{1,in}, T_{2,in}, T_{2.in,0}, T_{2.in,0}$	*(36)*	x_1, x_2
7	$n, \dot{m}_{1,0}, \dot{m}_{2,0}, T_{1.in,0}, T_{2.in,0}$	*(48)*	r
8	$r, n, \dot{m}_{1,0}, \dot{m}_{2,0}, x_1, x_2, \dot{m}_1, \dot{m}_2, (UA)_0$	*(38)*	UA
9	$\dot{m}_1\ , \dot{m}_2, c_p$	*(3), (5)* and *(9)*	$\dot{C}_1, \dot{C}_{2,}\dot{C}_{min}, \dot{C}_{max}, R_C$
10	$UA, \dot{C}_{min}$	*(7)*	NTU
11	$NTU, R_C, flow\ arrangement$	*(8)*	ε
12	$\dot{C}_{min}, \dot{C}_1, T_{1,in}, T_{2,in,}\varepsilon$	*(10)*	$T_{1,out}$
13	$\dot{C}_1, T_{1,in}, T_{1,out}$	*(11)*	$\dot{Q}$
14	$T_{2,in}, \dot{C}_2, \dot{Q}$	*(12)*	$T_{2,out}$

3.2.3 Flow Resistance Module

As mentioned above, the *flow resistance* sub-block implements the function of the *flow resistance* module. In Fig. 8, there are two *flow resistance* sub-blocks under the *E-NTU* block. They are used to calculate the pressure drops of two sides of the heat exchanger based on the mathematical model described in Section 2.2.2. The corresponding inputs, outputs, and applied equations of this module are listed in Table 5.

Table 5. Variables and equations of flow resistance module

Parameters: $T_{1,in,0}, T_{2,in,0}\ , \dot{m}_{1,0}, \dot{m}_{2,0}, , \Delta P_{1,0}, \Delta P_{2,0}, N$

Input Variables: $T_{1,in}, T_{2,in}, \dot{m}_1, \dot{m}_2$

No.	Input	Equation	Output
1	$T_{1,in,0}, T_{2,in,0}, T_{2,in}, T_{2,in}, \dot{m}_{1,0}, \dot{m}_{2,0}, N$	*(62)*	$x_{f,1}, x_{f,2}$
2	$x_{f,1}, x_{f,2}, \Delta P_{1,0}, \Delta P_{2,0}, \dot{m}_1, \dot{m}_2, N$	*(59)*	ΔP_1 , ΔP_2

4 Model Evaluation

In this section, the heat transfer module and the flow resistance module are evaluated separately as they are independent of each other. Two different methods are used to determine parameter n in the validation of the heat transfer module and parameter N in the validation of the flow resistance module. Parameter n was chosen from literature and parameter N was determined by calibration with the experimental data.

4.1 Evaluation of the Heat Transfer Module

4.1.1 Introduction of the Experimental Platform

The experimental data from the literature [48] are used to validate the proposed heat transfer module. Fig. 9 shows the system diagram of the experimental platform. The system consists of *Fan 1*, *Fan 2*, *Air heater*, *Dampers*, *PFHE* and a control system. The *Air heater* is used to raise the air inlet temperature on side 1. T-shape thermocouples are distributed evenly on the duct sections at the inlet and the outlet of the heat exchanger to acquire the average air temperature. The measurement accuracy is $\pm 0.1K$. Six hot-wire anemometers are installed evenly on the duct sections on both sides to obtain the average wind speed, with an accuracy of $\pm 0.05m/s$. The *PFHE* is a cross flow type with plain fins. We estimated the Reynolds number in this experiment lies approximately between 600 and 1700. The experimental results are listed in Table 6.

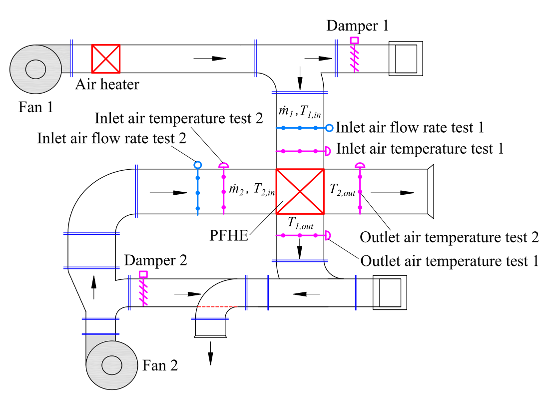

Fig. 9. System diagram of the experimental platform [48]

Table 6 Experiment results of PFHE [48]

Case	Air of side 1				Air of side 2				$\bar{\dot{Q}}$ (W)	Imbalance rate φ
	$\dot{m}_1$ (kg/s)	$T_{1,in}$ $(K$	$T_{1,out}$ (K)	$\dot{Q}_1$ (W)	$\dot{m}_2$ (kg/s)	$T_{2,in}$ (K)	$T_{2,out}$ (K)	$\dot{Q}_2$ (W)		
1	0.33	308.39	304.70	1230	0.33	300.30	304.09	1260	1245	2.44%
2	0.4	308.40	304.83	1440	0.4	300.20	303.62	1380	1410	4.17%
3	0.5	308.43	304.89	1790	0.5	300.42	303.83	1720	1755	3.91%
4	0.6	308.46	304.87	2180	0.6	300.32	303.78	2100	2140	3.67%
5	0.67	308.60	305.10	2370	0.67	300.40	303.73	2250	2310	5.06%
6	0.73	309.16	305.69	2560	0.73	300.34	303.76	2520	2540	1.56%
7	0.83	309.60	305.77	3210	0.83	300.50	304.16	3070	3140	4.36%

Note: 1) $\bar{\dot{Q}}$ is mean value of $\dot{Q}_1$ and $\dot{Q}_2$; 2) the definition of imbalance is: $\varphi = \frac{|\dot{Q}_1 - \dot{Q}_2|}{\dot{Q}_1} \times 100\%$.

4.1.2 Validation Results

As mentioned before, the range of Reynolds number in this experiment is approximately 600~1700 and the fin is plain fin. According to Table 2, we chose the exponent m of the heat transfer factor j from the literature [6]: $m = -0.3345, n = m + 1 = 0.6655$. As mentioned in Section 2.1, the nominal condition is definite and decided by the users in design phase. Here, from Table 6, we chose Case 6 of minimum imbalance rate as the nominal condition and the corresponding nominal parameters are: $\dot{Q}_0 = 2540W, \dot{m}_{1,0} = 0.73kg/s, \dot{m}_{2,0} = 0.73kg/s, T_{1,in,0} = 309.16K, T_{2,in,0} = 300.34K$. We define the non-dimensional outlet temperature $\vartheta_{1,out}$ on side 1 and $\vartheta_{2,out}$ on side 2 as:

$$\vartheta_{1,out} = \frac{T_{1,in} - T_{1,out}}{T_{1,in} - T_{2,in}}, \quad (63)$$

and

$$\vartheta_{2,out} = \frac{T_{2,out} - T_{2,in}}{T_{1,in} - T_{2,in}}, \quad (64)$$

respectively. The simulation results are shown in Fig. 10~Fig. 12.

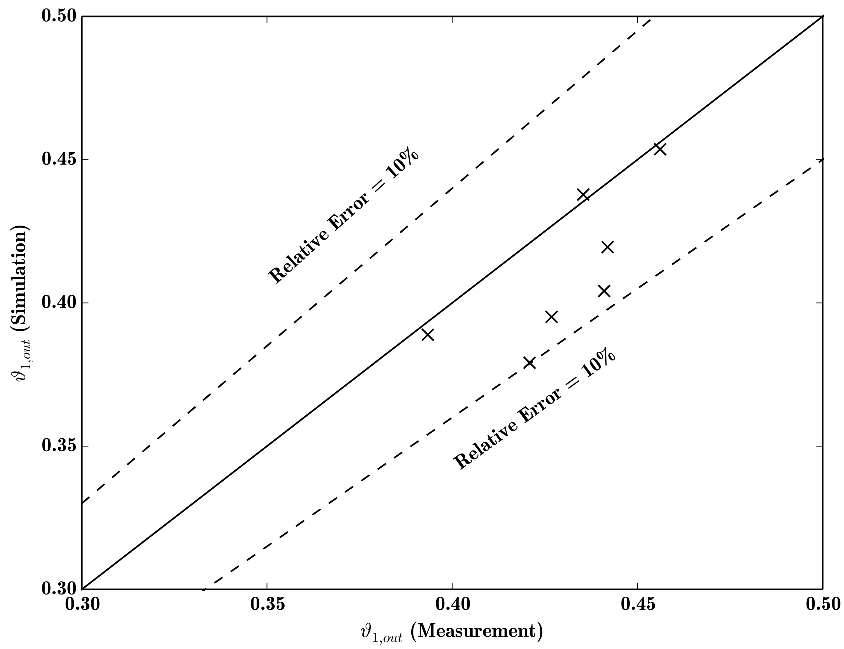

Fig. 10. Comparison of $\vartheta_{1,out}$ between simulation and measurement

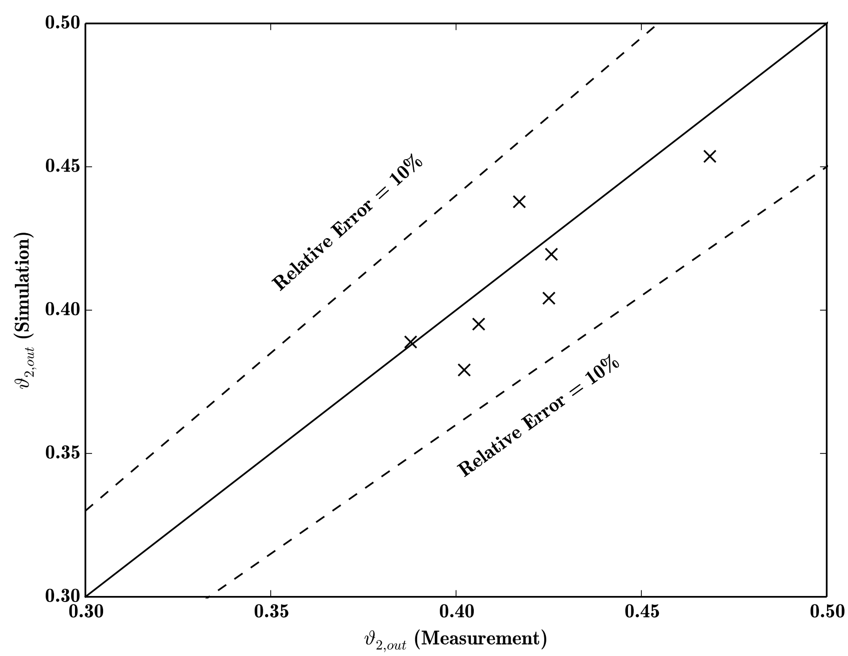

Fig. 11. Comparison of $\vartheta_{2,out}$ between simulation and measurement

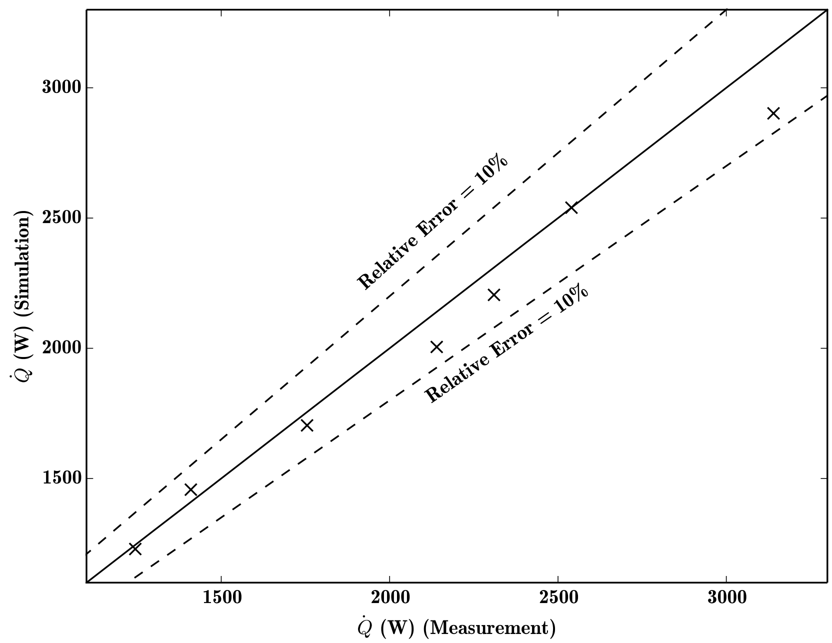

Fig. 12. Comparison of $\dot{Q}$ between simulation and measurement

Fig. 10 shows the comparison of the non-dimensional outlet temperature $\vartheta_{1,out}$ on side 1 between simulation results and the measurements. It can be seen from the figure that the differences between simulation and measurement are small and the largest deviation occurs at Case7, where the absolute deviation of $\vartheta_{1,out}$ is 0.042 and the relative deviation is 9.92%. Fig. 11 shows the comparison of the non-dimensional outlet temperature $\vartheta_{2,out}$ on side 2. The largest deviation occurs at Case 7, where the absolute deviation of $\vartheta_{2,out}$ is 0.023 and the relative deviation is 5.74%. As can be seen from Fig. *10* and Fig. *11*, some cases (e.g. Case 3~5 in Fig. *10*, Case 4 and 7 in Fig. *11*) show larger deviations of $\vartheta_{1,out}$ and $\vartheta_{2,out}$ between the simulation results and the measurements. The reason lies in that in the model, the calculation of $\vartheta_{1,out}$ and $\vartheta_{2,out}$ is dependent on four temperature variables: $T_{1,in}$, $T_{2,in}$, $T_{1,out}$ and $T_{2,out}$. The errors of the simulation results of the four variables might accumulate during the calculation of the non-dimensional outlet temperatures. On the other hand, the measurement data used to validate the model are obtained by experimental equipment, which usually have systematic error and random error. Hence, it is difficult to ensure the consistency between the simulation results and the measurements for each case. However, generally speaking, the relative deviation of the simulation results from the experimental data is controlled within 10%. Fig. 12 shows the comparison of heat transfer $\dot{Q}$

between simulation results and experimental results $\bar{\dot{Q}}$. $\bar{\dot{Q}}$ is the mean value of heat transfer on both sides of the heat exchanger. It is indicated by the figure that the difference between the simulation and the experiment is small. The largest deviation occurs at Case 7, where the absolute deviation of heat transfer is $238W$ and the relative deviation is 7.58%. As shown in the above results, the heat transfer module simulates PFHEs with a relative deviation smaller than 10%.

4.2 Evaluation of the Flow Resistance Module

4.2.1 Introduction of the Experimental Platform

The experimental data from the literature [36] are used to validate the proposed flow resistance module. The PFHE used in the experiment consists of plain fins in hot-pass and wavy fins in cold-pass. The air pressure on the hot-side is far beyond 1 bar, which goes beyond the pressure scope of the resistance module in this paper. Hence, we only used the experimental data for the cold side to validate the module. Fig. 13 shows the scheme of the wind tunnel of cold-pass as the experimental platform. The component *Pressure difference test* is used to test the pressure drop Dp in the PFHE. The inlet and outlet pressures are measured by pressure sensors with a tolerance of ±0.25%. The temperature measuring nets with a standard uncertainty of $\pm 0.5K$. The whole measurement uncertainty lies in the range of −2% ~ +2%. The experimental results of the cold pass are listed in Table 7.

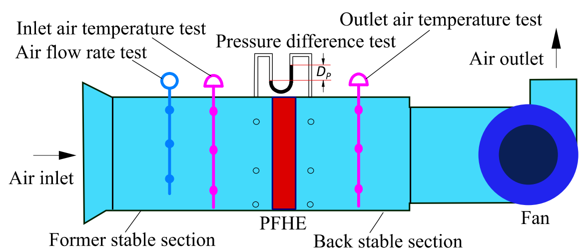

Fig. 13. Experimental platform [36]

Table 7 Experiment results of the cold pass (wavy fins) [36]

Case	**Air velocity V (m/s)**	**Flow rate $\dot{m}$ (kg/s)**	**Inlet temperature $T_{in}(K)$**	**Pressure drop $Dp(Pa)$**
1	2.0	0.219	285.25	11.00
2	4.5	0.492	287.55	36.00

3	2.0	0.219	288.05	11.00
4	4.5	0.492	288.65	36.00
5	8.0	0.876	289.15	85.00
6	2.0	0.219	288.05	11.00
7	8.0	0.876	288.55	85.00
8	4.5	0.492	287.55	35.00
9	8.0	0.876	287.85	84.00

4.2.2 Calibration

Instead of choosing the friction factor exponent N from literature, we used part of the measurements in Table 7 to calibrate the value of N, so that the simulation results better fit the experimental results. As mentioned in Section 2.1, the nominal condition is definite and decided by the users in design phase. Here, we select one of these conditions of maximum mass flow rate as nominal condition. From Table 7, we chose Case 9 as the nominal condition. The nominal parameters are as follows: $\dot{m}_0 = 0.876kg/s$, $T_0 = 287.85K$, $Dp_0 = 84Pa$. Then, Case 1~Case 4 were used to calibrate N. Substituting the flow rate, inlet temperature and pressure drop of each chosen case and the nominal data into *Eq. (59)* and *Eq. (62)*, we can get the N value in each chosen case. Calculating the average of these four N values, we get the calibrated N value of -0.5315.

4.2.3 Validation Results

Case 5~Case 8 were used to validate the flow resistance module. The validation results are shown in Fig. 14. From the figure, we can see that the simulation results of pressure drop Dp are close to the experimental data. The largest deviation occurs at Case 8, where the absolute deviation is 1.03 Pa and the relative deviation is 2.96%. So, we can conclude that the proposed flow resistance module simulates the PFHE with a reasonable relative deviation.

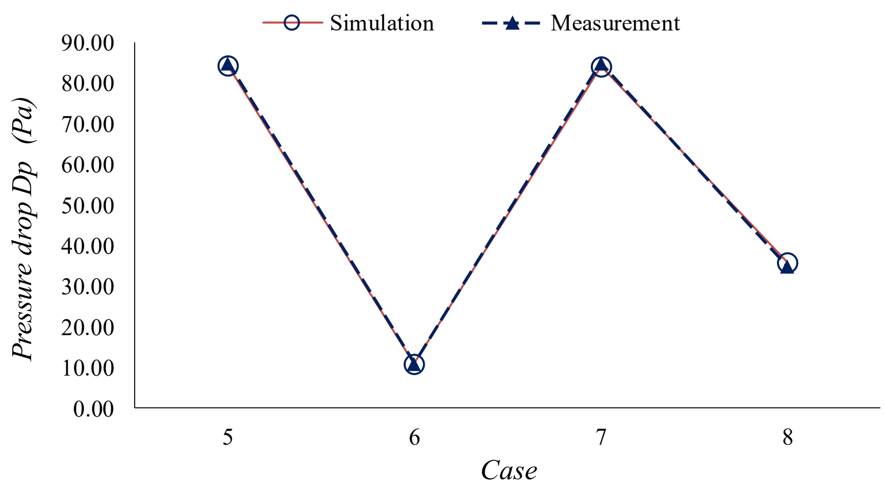

Fig. 14. Comparison of Dp between simulation and measurement

5 Conclusion

In this paper, a new air-to-air PFHE model is proposed, which can calculate both heat transfer and flow resistance. Mathematical models for the two parts are first built. Then, the model is using the object-oriented language Modelica. Existing experimental data from the literature are used to evaluate the heat transfer module and the flow resistance module, respectively. The results show that the new model can simulate air-to-air PFHEs within reasonable deviation.

This new model considers the impact of the changing air flow rate and temperature. It is capable of predicting part-load behavior with only nominal data, which are accessible in the design phase. The new model does not need geometric data as inputs or require numerical discretization, which makes it computationally more efficient than models using finite-element method. Besides plate-fin heat exchangers, the new model can be used to calculate the heat transfer of other kinds of air-to-air heat exchangers, if only the correlations have the form of $j= c_1 c_2 Re^m$ or $Nu = CRe^n$ and no dehumidification is considered. Similarly, it can also calculate the pressure drop of other kinds of air-to-air heat exchangers, if only the correlations have the following form: $f= k_1 k_2 Re^N$ and $f = (A_{min}/A)(2\,\Delta P/\rho u^2)$.

So far, this new model can only be applied for dry conditions. As the next step, the PFHE model with dehumidification will be developed.

Acknowledgement

This work was supported by the National Science Foundation of USA [No. IIS-1802017] and a special fund for energy saving research from the government of Guangzhou in China [No. J-2016-11]. The authors want to thank Dr. Michael Wetter at the Lawrence Berkeley National Laboratory who provided constructive comments and suggestions for this paper.

References

[1] Y. Deng, Z. Feng, J. Fang, S.J. Cao, Impact of ventilation rates on indoor thermal comfort and energy efficiency of ground-source heat pump system, Sustainable Cities & Society, 37 (2018) 154-163.

[2] C. Ren, Y. Deng, S.J. Cao, Evaluation of polyethylene and steel heat exchangers of ground source heat pump systems based on seasonal performance comparison and life cycle assessment, Energy & Buildings, 162 (2018).

[3] M.K. Kim, J. Liu, S.J. Cao, Energy analysis of a hybrid radiant cooling system under hot and humid climates: A case study at Shanghai in China, Building & Environment, 137 (2018) 208-214.

[4] M. Picon-Nunez, G. Polley, E. Torres-Reyes, A. Gallegos-Munoz, Surface selection and design of plate–fin heat exchangers, Applied Thermal Engineering, 19 (1999) 917-931.

[5] L.S. Ismail, R. Velraj, C. Ranganayakulu, Studies on pumping power in terms of pressure drop and heat transfer characteristics of compact plate-fin heat exchangers—A review, Renewable and Sustainable Energy Reviews, 14 (2010) 478-485.

[6] J.Q. Dong, Research on Air Side Flow and Heat Transfer Character of Vehicle Cooling Systems, in, Vol. Ph.D. Thesis, Shanghai Jiaotong University, Shanghai, China, 2007.

[7] M. Khoshvaght-Aliabadi, F. Hormozi, A. Zamzamian, Role of channel shape on performance of plate-fin heat exchangers: Experimental assessment, International Journal of Thermal Sciences, 79 (2014) 183-193.

[8] L.S. Zhang Xiaosong, Zhao Kaitao,Chen Jiming, Research on energy recovery from exhaust air using plate-fin heat exchanger in air conditioning system, Ventilation and Dust Removal (1998) 4-7.

[9] M. Wetter, Air-to-Air Plate Heat Exchanger, Simulation Research Group Building technologies Department Environmental Energy technologies Division Lawrence Berkeley National Laboratory Berkeley, CA, 94720 (1999).

[10] K. Nakonieczny, Numerical modeling of cross-flow plate-fin air-to-air heat exchanger under unsteady flow conditions, Numerical Heat Transfer, Part A: Applications, 49 (2006) 1-24.

[11] S.J. Cao, X.R. Kong, Y. Deng, W. Zhang, L. Yang, Z.P. Ye, Investigation on thermal performance of steel heat exchanger for ground source heat pump systems using full-scale experiments and numerical simulations, Applied Thermal Engineering, 115 (2017) 91-98.

[12] X.R. Kong, Y. Deng, L. Li, W.S. Gong, S.J. Cao, Experimental and numerical study on thermal performance of ground source heat pump with a set of designed buried pipes, Applied Thermal Engineering, 114 (2016) 110-117.

[13] J. Rose, T.R. Nielsen, J. Kragh, S. Svendsen, Quasi-steady-state model of a counter-flow air-to-air heat-exchanger with phase change, Applied Energy, 85 (2008) 312-325.

[14] T.R. Nielsen, J. Rose, J. Kragh, Dynamic model of counter flow air to air heat exchanger for comfort ventilation with condensation and frost formation, Applied Thermal Engineering, 29 (2009) 462-468.

[15] P. Liu, M. Rafati Nasr, G. Ge, M. Justo Alonso, H.M. Mathisen, F. Fathieh, C. Simonson, A theoretical model to predict frosting limits in cross-flow air-to-air flat plate heat/energy exchangers, Energy and Buildings, 110 (2016) 404-414.

[16] M. Wetter, W. Zuo, T.S. Nouidui, X. Pang, Modelica buildings library, Journal of Building Performance Simulation, 7 (2014) 253-270.

[17] DoE, EnergyPlus™ Version 8.6 Documentation_Engineering Reference, in, 2016.

[18] S. Klein, W. Beckman, J. Mitchell, J. Duffie, N. Duffie, T. Freeman, J. Mitchell, J. Braun, B. Evans, J. Kummer, et al, TRNSYS 17. A TRaNsient SYstem Simulation Program; Mathematical Reference, Solar Energy Laboratory, University of Wisconsin-Madison: Madison, WI, USA, 4 (2014).
[19] S. Klein, W. Beckman, J. Mitchell, J. Duffie, N. Duffie, T. Freeman, J. Mitchell, J. Braun, B. Evans, J. Kummer, et al, TRNSYS 18. A TRaNsient SYstem Simulation Program; Standard Component Library Overview, Solar Energy Laboratory, University of Wisconsin-Madison: Madison, WI, USA, 3 (2017).
[20] J. Thornton, D. Bradley, T. McDowell, N. Blair, M. Duffy, N. LaHam, A. Naik, et al, TESSLibs 17 HVAC Library Mathematical Reference, Thermal Energy System Specialists, Madison, Wisconsin, (2014).
[21] M. Wetter, Modelica library for building heating, ventilation and air-conditioning systems, Lawrence Berkeley National Laboratory, (2010).
[22] R.M. Manglik, A.E. Bergles, Heat transfer and pressure drop correlations for the rectangular offset strip fin compact heat exchanger, Experimental Thermal and Fluid Science, 10 (1995) 171-180.
[23] R.K. Shah, D.P. Sekulic, Fundamentals of heat exchanger design, John Wiley & Sons, 2003.
[24] S. Tan, The Application for Design Optimization of the Plate-Fin Heat Exchanger Based on Genetic Algorithm, in, Vol. Master's thesis, Anhui University of Technology Ma anshan, China, 2013.
[25] M. Wetter, Simulation model finned water-air-coil withoutcondensation, in, Ernest Orlando Lawrence Berkeley National Laboratory, Berkeley, CA (US), 1999.
[26] Y.-J. Chang, C.-C. Wang, Air side performance of brazed aluminum heat exchangers, Journal of Enhanced Heat Transfer, 3 (1996).
[27] Y.-J. Chang, C.-C. Wang, A generalized heat transfer correlation for Iouver fin geometry, International Journal of heat and mass transfer, 40 (1997) 533-544.
[28] M.-H. Kim, C.W. Bullard, Air-side thermal hydraulic performance of multi-louvered fin aluminum heat exchangers, International Journal of Refrigeration, 25 (2002) 390-400.
[29] L.S. Ismail, R. Velraj, Studies on Fanning friction (f) and Colburn (j) factors of offset and wavy fins compact plate fin heat exchanger–a CFD approach, Numerical Heat Transfer, Part A: Applications, 56 (2009) 987-1005.
[30] R.B.S. Rao, G. Ranganath, C. Ranganayakulu, Development of colburn ‘j’factor and fanning friction factor ‘f’correlations for compact heat exchanger plain fins by using CFD, Heat and Mass Transfer, 49 (2013) 991-1000.
[31] D. Mohan, K.S. Moorthy, S.S.S. Sivam, S. Rajendrakumar, Experimental Investigation of Heat Transfer Study on Plate Fin Heat Exchangers with Wavy Fins, Indian Journal of Science and Technology, 9 (2016).
[32] J. Dong, J. Chen, Z. Chen, W. Zhang, Y. Zhou, Heat transfer and pressure drop correlations for the multi-louvered fin compact heat exchangers, Energy Conversion & Management, 48 (2007) 1506-1515.
[33] J. Dong, J. Chen, Z. Chen, Y. Zhou, W. Zhang, Heat transfer and pressure drop correlations for the wavy fin and flat tube heat exchangers, Applied Thermal Engineering, 27 (2007) 2066-2073.
[34] K. Aliabadi, G. Samani, Hormozi, H. Asl, 3D-CFD simulation and neural network model for the j and f factors of the wavy fin-and-flat tube heat exchangers, Brazilian Journal of Chemical Engineering, 28 (2011) 505-520.
[35] F. Hormozi, E.H. Rad, M.K. Aliabadi, New correlations for wavy plate-fin heat exchangers: different working fluids, International Journal of Numerical Methods for Heat & Fluid Flow, 24 (2014) 1086-1108.
[36] Y. Huang, Z. Liu, G. Lu, X. Yu, Multi-scale thermal analysis approach for the typical heat exchanger in automotive cooling systems, International Communications in Heat and Mass Transfer, 59 (2014) 75-87.
[37] L. Zhiwei, Fundamentals & Equipment of Heat & Mass Transfer, 3 ed., China Building Industry Press, Beijing,China, 2011.
[38] A.R. Wieting, Empirical correlations for heat transfer and flow friction characteristics of rectangular offset-fin plate-fin heat exchangers, Journal of Heat transfer, 97 (1975) 488-490.
[39] M. Wetter, M. Bonvini, T.S. Nouidui, Equation-based languages–A new paradigm for building energy modeling, simulation and optimization, Energy and Buildings, 117 (2016) 290-300.
[40] M. Wetter, Modelica-based modelling and simulation to support research and development in building energy and control systems, Journal of Building Performance Simulation, 2 (2009) 143-161.

[41] M. Wetter, M. Bonvini, T.S. Nouidui, W. Zuo, Modelica Buildings library 2.0, in: Proc. of The 14th International Conference of the International Building Performance Simulation Association (Building Simulation 2015), Hyderabad, India, 2015.
[42] W. Tian, T.A. Sevilla, W. Zuo, M.D. Sohn, Coupling fast fluid dynamics and multizone airflow models in Modelica Buildings library to simulate the dynamics of HVAC systems, Building and Environment, (2017).
[43] W. Zuo, M. Wetter, W. Tian, D. Li, M. Jin, Q. Chen, Coupling indoor airflow, HVAC, control and building envelope heat transfer in the Modelica Buildings library, Journal of Building Performance Simulation, 9 (2016) 366-381.
[44] S. Huang, A.C.L. Malara, W. Zuo, M.D. Sohn, A Bayesian network model for the optimization of a chiller plant's condenser water set point, Journal of Building Performance Simulation, (2016) 1-12.
[45] S. Huang, W. Zuo, M.D. Sohn, Amelioration of the cooling load based chiller sequencing control, Applied Energy, 168 (2016) 204-215.
[46] S. Huang, W. Zuo, M.D. Sohn, Improved cooling tower control of legacy chiller plants by optimizing the condenser water set point, Building and Environment, 111 (2017) 33-46.
[47] R. Miranda, S. Huang, G. Barrios, D. Li, W. Zuo, Energy efficient design for hotels in the tropical climate using Modelica, in: 11th International Modelica Conference, Versailles, France, September 21-23, 2015, Linköping University Electronic Press, 2015, pp. 71-78.
[48] G. Gao, Applicability study of the spray indirect evaporative cooling in the Yangtze River valley, in, Vol. Master's thesis, Chongqing University, Chongqing, China, 2008.